

RESEARCH PAPER



Carbonic anhydrase 12 mutation modulates membrane stability and volume regulation of aquaporin 5

Soyoung Hwang^{a*}, Jung Yun Kang^{b*}, Min Jae Kim^b, Dong Min Shin^b and Jeong Hee Hong^{a,c}

^aDepartment of Physiology, College of Medicine, Gachon University, Incheon, Republic of Korea; ^bDepartment of Oral Biology, BK21 PLUS Project, College of Dentistry, Yonsei University, Seoul, Republic of Korea; ^cDepartment of Health Sciences and Technology, GAIHST, Gachon University, Incheon, Republic of Korea

ABSTRACT

Patients carrying the carbonic anhydrase12 E143K mutation showed the dry mouth phenotype. The mechanism underlying the modulation of aquaporin 5 and function in the salivary glands by carbonic anhydrase12 remains unknown. In this study, we identified the mislocalised aquaporin 5 in the salivary glands carrying the E143K. The intracellular pH of E143K cells was more acidic than that of the cells carrying wild type. To evaluate the role of carbonic anhydrase12 on the volume regulation of aquaporin 5, the submandibular gland cells were subjected to hypotonic stimuli. E143K enhanced the extent of swelling of cells on hypotonicity. Aquaporin 5 modulates water influx through ion transporters to prevent osmotic imbalance. These results suggest that the carbonic anhydrase12 E143K, including acidification or inflammation, mediates volume dysregulation by the loss of aquaporin 5. Thus, carbonic anhydrase12 may determine sensible effects on the cellular osmotic regulation by modulating aquaporin 5.

ARTICLE HISTORY

Received 9 September 2018
 Revised 19 October 2018
 Accepted 22 October 2018

KEYWORDS

Carbonic anhydrase 12; aquaporin 5; volume regulation; acidosis; salivary glands

Introduction

Aquaporin 5 (AQP5) is a member of the transmembrane protein channels involved in transcellular water permeability and a dominant water channel in the epithelia of the salivary and lacrimal glands and the lung alveoli^{1,2}. A study using AQP5 knockout mice showed that AQP5 plays a central role in salivary secretion³. Indeed, AQP5 classically prevents excessive water reabsorption and modulates cell shape and volume⁴. Recently, several new roles of AQP5, in addition to water transport, have been discussed. AQP5 is involved in migration by activating Ras and Rac signalling in cancer cells⁵ and is associated with cancer cell invasion and tumour metastasis through the NF- κ B signalling pathway⁶. Additionally, hyperosmotic stress-mediated AQP5 expression mediates the expression of inflammatory cytokines and cell death through the JNK1/2 MAPK signalling pathway⁷.





The *in vitro* trafficking of AQP5 from the intracellular segments to the plasma membrane was mediated by secretory stimulation caused by factors such as acetylcholine¹. However, *in vivo* evidence for the trafficking of AQP5 remains unknown. We focused on patients carrying the carbonic anhydrase 12 (CA12) E143K point mutation who showed dry mouth phenotype⁸. In addition, in the *ex vivo* mouse model, the volume of saliva secreted from the salivary glands of CA12 E143K (E/K)-mutated mice was dramatically reduced by using the adenovirus-mediated CA12 E/K gene transfer system⁸. Downregulated activities of the electrogenic sodium-bicarbonate co-transporter 1-B (NBCe1-B) and anion exchanger 2 (AE2) could be partially responsible for the reduced salivary volume caused by the CA12 E/K mutation.

The higher electrolyte concentration caused by the CA12 E/K mutation indicated reduced water volume⁸. CA12 is a basolateral membrane-associated enzyme, which possesses the catalytic site at the extracellular surface, regulating extracellular HCO₃⁻ concentration⁹. Typically, the membrane channels of exocrine glands such as salivary glands are localised with polarisation. AQP5 is expressed at and localised to the luminal membrane of acinar cells¹⁰. However, the association between CA12 mutation and reduced salivary volume remains unknown. In our previous study, we showed that the CA12 mutation mediates abnormal localisation of CA12 in the cytosol⁸. CAs generate the acidic component, CO₂, as well as the pH buffer ion HCO₃⁻⁹. The cytosolic expression of CA12 E/K mutation can be expected to be modulated by the intracellular pH (pH_i). CA12 mutation-induced modulation of the water channel AQP5 might provide an evidence of reduced salivary function. In this study, we found the presence of mislocalised AQP5 in the CA12 E/K-mutated salivary glands *in vivo*. Thus, to examine whether CA12 and AQP5 physically associate in the salivary glands, we designed this study to assess the effects of CA12 and its E/K mutant on the expression and volume regulation of AQP5. Here, we address the definitive mechanism employed by CA12 and its mutant on the volume regulation of AQP5 with respect to the physiological conditions in the exocrine glands.


Material and methods

Reagents and plasmids

β -Actin antibody (A3854), 4,4'-diisothiocyano-2,2'-stilbenedisulfonic acid (DIDS; 462268), carbachol (1092009), acetazolamide (A6011),

CONTACT Dong Min Shin  dmsin@yuhs.ac  Department of Oral Biology, BK21 PLUS Project, Yonsei University College of Dentistry, Seoul 03722, Republic of Korea; Jeong Hee Hong  minicleo@gachon.ac.kr  Department of Physiology, College of Medicine, Gachon University, 155 Getbeolro, Yeonsu-gu, Incheon 21999, Republic of Korea

*These authors contributed equally to this work.

 Supplemental data for this article can be accessed [here](#).

© 2018 The Author(s). Published by Informa UK Limited, trading as Taylor & Francis Group.

This is an Open Access article distributed under the terms of the Creative Commons Attribution License (<http://creativecommons.org/licenses/by/4.0/>), which permits unrestricted use, distribution, and reproduction in any medium, provided the original work is properly cited.

and amiloride hydrochloride hydrate (Amiloride; A7410) were purchased from Sigma (Saint-Louis, MO). AQP5 (ab92320), Na⁺-K⁺-Cl⁻ co-transporter1 (NKCC1, ab59791), SLC26A6 (ab123001), and AE2 (ab42687) antibodies were purchased from Abcam (Cambridge, MA). CA12 antibody was purchased from ProteinTech Inc. (15180-1-AP; Chicago, IL). 2',7'-Bis-(carboxyethyl)-5-(and-6)-carboxyfluorescein (BCECF)-AM was purchased from TEF labs (0061; Austin, TX). TNF- α (210-TA-005) was purchased from R&D Systems (Minneapolis, MN). Calcein-AM was purchased from Molecular Probes (C1430; Eugene, OR). Pluronic acid (F-127, 20% in dimethyl sulphoxide, P-3000MP), pHrodo Green AM (P35373), and ZO-1 antibody (940-2200) were purchased from Invitrogen (Carlsbad, CA). All other chemicals were purchased from Sigma. GFP-tagged human AQP5 was a kind gift from Kyung Pyo Park (Seoul National University, South Korea), and DNA plasmids for pcDNA3.0-human NKCC1, mKate-human SLC26A6, HA-rabbit AE2, mKate-human CA12 wild type, and mKate-CA12 E143K mutants were generously provided by Dr. Shmuel Muallem (National Institutes of Health, Bethesda)⁸.

Cell culture

Human embryonic kidney 293 T cells (HEK293T) was maintained in Dulbecco's modified Eagle's medium (Invitrogen, 11995-065) containing 10% fetal bovine serum (FBS; Invitrogen, 16000-044), and 100 U/mL penicillin-streptomycin (Invitrogen, 15140-122) and incubated at 37 °C in a humidified environment containing 5% CO₂ and 95% air. When the cells reached 80% confluency, the culture medium was aspirated, and the cells were washed with Dulbecco's phosphate-buffered saline (DPBS, Welgene, South Korea, LB001-02), followed by their treatment with trypsin/ethylenediaminetetraacetic acid (EDTA) for 2 min. The dispersed cells were transferred to new culture dishes for western blotting and co-immunoprecipitation (Co-IP) or to culture dishes with glass coverslips for imaging.

Isolation of mouse submandibular glands (SMG) acinar cells

All experimental protocols for animals and their maintenance and care were undertaken according to the Gachon University Animal Care guidelines. All animal procedures were approved by the Center of Animal Care and Use, Lee Gil Ya Cancer and Diabetes Institute, Gachon University, and the Institutional Animal Care and Use Committee (IACUC) (Permission number: LCDI-2017-0014). Mouse SMG cells were isolated from 22–25 g C57BL/6 mice, and the isolated tissues and cells were suspended in physiological salt solution A (PSA; 140 mM sodium chloride [NaCl], 10 mM glucose, 5 mM potassium chloride [KCl], 1 mM magnesium chloride [MgCl₂], 1 mM calcium chloride [CaCl₂], 10 mM HEPES [pH 7.4], 0.02% soybean-trypsin inhibitor, 0.1% sodium pyruvate, and 0.1% bovine serum albumin [BSA]), and stored on ice until use. The isolated tissues were minced with scissors and incubated in collagenase P solution (2.5 mg/10 ml in PSA; Roche) for 6 min at 37 °C with vigorous shaking. The isolated acinar cells were washed and re-suspended in PSA and stored on ice until use.

Adenovirus-transduced mice

To overexpress the CA *in vivo*, the adenovirus (Ad)-transduced mice were developed as previously described⁸. Briefly, the CA12 and CA12 E143K fragments were generated by PCR and ligated into pAC-IRES-RFP to generate pAC-CA12-IRES-RFP and pAC-CA12 E/K. Adenoviruses were delivered to 8-week-old C57BL/6 mice.

The mice were anaesthetised with the both SMG and parotid glands cannulated. Saline (50 μ L for the SMG glands) containing AdCA12 or AdCA12 E/K (5 \times 10⁹ particles per gland) was then administered by retrograde ductal instillation. After 7 days, the SMG were isolated and dissected for immunostaining.

Measurement of CBE and NKCC activities

Isolated SMG cells were attached onto coverslips and loaded in the chamber containing 6 μ M BCECF-AM in the presence of 0.05% pluronic acid (F-127) in HEPES-buffered solution (Table 1) for 15 min at room temperature. After stabilisation of the fluorescence, the cells were perfused with solution A for a minimum of 5 min prior to measuring the pH_i. The pH_i was measured by BCECF fluorescence at dual excitation wavelengths of 495 and 440 nm and an emission wavelength of 530 nm. The chloride/bicarbonate exchange (CBE) activity of AE2 and SLC26A6 was determined using Cl⁻-free HCO₃⁻-buffered solution (Table 2) containing 126 mM Na⁺. The cells were incubated with CO₂-saturated HCO₃⁻-buffered solution (Table 3) for the acidification of the cytosol, and then perfused with Cl⁻-free HCO₃⁻-buffered solution. CBE activity was calculated from the slope of increase in pH_i during the first 30–45 s in Cl⁻-free HCO₃⁻-buffered solution and expressed as percent fold change relative to that of the CBE activity of the control. NKCC1 activity was estimated from the slope of change in pH_i by using 10 mM NH₄Cl in HEPES-buffered solution. Administration of NH₄Cl in the extracellular solution induced initial alkalinisation by the diffusion of NH₃, and then, pH_i was decreased by NH₄⁺ influx, as a substitution of K⁺. The pH_i recovery rate in the second phase provides NH₄⁺ influx. The traces were normalised at the time point of NH₄Cl administration. The slope of second-phase acidification was calculated and represented as a ratio. To mimic intracellular acidification, the isolated SMG cells were treated with Na⁺-free solution (0Na⁺, Table 4) and Amiloride, a sodium channel inhibitor, followed by 10 mM NH₄Cl stimulation. Images were obtained at 1-s interval by using a CCD camera (Retiga 6000; Q-Imaging, Canada) linked to an inverted microscope (Olympus, Japan), and analysed with a MetaFluor system (Molecular Devices, PA). Each image was normalised by subtracting the background fluorescence from the raw background signals.

Table 1. Composition of HEPES-based solution.

Composition	Final concentration
Sodium chloride (NaCl)	140 mM
HEPES	10 mM
Glucose	10 mM
Potassium chloride (KCl)	5 mM
Magnesium chloride (MgCl ₂)	1 mM
Calcium chloride (CaCl ₂)	1 mM
	pH 7.4
	300mOsm (310 for SMG)

Table 2. Composition of Cl⁻-free HCO₃⁻-buffered solution.

Composition	Final concentration
Sodium gluconate	120 mM
HEPES	2.5 mM
Glucose	10 mM
Potassium gluconate	5 mM
Magnesium sulfate (MgSO ₄)	1 mM
Calcium gluconate	0.5 mM
Sodium bicarbonate (NaHCO ₃)	25 mM
	pH 7.8
	310 mOsm

Table 3. Composition of HCO₃⁻-buffered solution.

Composition	Final concentration
Sodium chloride (NaCl)	120 mM
HEPES	2.5 mM
Glucose	10 mM
Potassium chloride (KCl)	5 mM
Magnesium chloride (MgCl ₂)	1 mM
Calcium chloride (CaCl ₂)	1 mM
Sodium bicarbonate (NaHCO ₃)	25 mM
pH 7.8	
300mOsm (310 for SMG)	

Table 4. Composition of Na⁺-free solution.

Composition	Final concentration
NMDG-Cl (pH ≥7.4)	125 mM
HEPES	2.5 mM
Glucose	10 mM
Potassium chloride (KCl)	5 mM
Magnesium chloride (MgCl ₂)	1 mM
Calcium chloride (CaCl ₂)	1 mM
adjusting pH to 7.8 (with. Choline Bicarbonate)	
310 mOsm	

Cell acidification

To mimic intracellular acidification, the isolated SMG cells were treated with 10 mM NH₄Cl in the extracellular solution induced initial alkalinisation for 1 min and subsequently treated with ONa⁺ and Amiloride, a sodium channel inhibitor, for indicated times. Treated SMG cells were used in the biotinylated assay, pH imaging, and confocal imaging.

DNA transfection

Plasmid DNAs (Total amount of DNA: 2 μg) were incubated in 200 μL of Opti-Eagle's minimum essential medium (Opti-MEM™; Invitrogen, 31985-070) and mixed with the Lipofectamine 2000 mixture. The mixture was incubated at room temperature for 25 min and transferred into cell dishes containing culture medium. After 4 h, the transfected medium was replaced with the fresh culture medium, and the cells were used at 24 h after transfection. Plasmid DNA transfection by Lipofectamine 2000 was performed according to the manufacturer's protocol (Invitrogen, 11668019).

Measurement of volume changes

The transfected cells and isolated SMG cells were loaded with 2 μM calcein-AM (Molecular Probes) in the presence of 0.01% pluronic acid (F-127) for 15 min at room temperature. After stabilisation of fluorescence, the cells were perfused with HEPES-buffered solution for a minimum of 5 min prior to volume measurement. The calcein-AM dye was excited at 495 nm, and the emitted fluorescence was measured at 515 nm. Cell volume was determined using a hypotonic (215 mOsm, Table 5) or hypertonic (500 mOsm, Table 6) solution. Fluorescence images were captured at 1-s interval by using a CCD camera (Retiga 6000, Q-Imaging, Canada) linked to an inverted microscope (Olympus, Japan), and analysed with a MetaFluor system (Molecular Devices, PA). Each image was normalised by subtracting the background fluorescence from the raw background signals.

Co-immunoprecipitation, surface biotinylation and Western blotting

Transfected cells were incubated with lysis buffer (Cell Signaling, 9803) containing 20 mM Tris, 150 mM NaCl, 2 mM EDTA, 1% Triton

Table 5. Composition of hypotonic-buffered solution.

Composition	Concentration
Sodium chloride (NaCl)	80 mM
HEPES	10 mM
Glucose	10 mM
Potassium chloride (KCl)	5 mM
Magnesium chloride (MgCl ₂)	1 mM
Calcium chloride (CaCl ₂)	1 mM
pH 7.4	
215 mOsm	

Table 6. Composition of hypertonic-buffered solution.

Composition	Concentration
Sodium chloride (NaCl)	140 mM
HEPES	10 mM
Glucose	10 mM
Potassium chloride (KCl)	5 mM
Magnesium chloride (MgCl ₂)	1 mM
Calcium chloride (CaCl ₂)	1 mM
pH 7.4	
500 mOsm	

X-100, and a protease inhibitor mixture for 5 min at room temperature. The cells were sonicated and centrifuged at 11,000 ×g for 15 min at 4 °C and protein concentration was determined by Bradford assay (Bio-Rad, Hercules, CA). For Co-IP, the lysate was treated with 1 μg/mL of the indicated antibodies at 4 °C for 16 h with gentle shaking and added protein G plus agarose beads (Santa Cruz, SC-2002) for 4 h. The beads were centrifuged at 11,000 ×g for 2 min at 4 °C and discard the supernatant and washed thrice with the lysis buffer at 4 °C. The beads were incubated in the sample buffer at 37 °C for 15 min for protein detachment. Eluted proteins were applied in western blotting. To demonstrate the surface expression of proteins, the transfected cells were incubated with 0.5 mg/mL EZ-LINK Sulfo-NHS-LC-biotin (Thermo, 21335) for 30 min on ice, and then treated with 100 mM cold glycine solution (in PBS) for 10 min. The incubated cells were washed thrice with PBS buffer and incubated with the lysis buffer. Cell extracts were centrifuged at 11,000 ×g for 15 min at 4 °C. The supernatants were incubated overnight with Avidin beads (Thermo, 20347) at 4 °C and the beads were washed with the lysis buffer. Collected beads were heated at 37 °C for 15 min in the presence of the sample buffer to recover proteins. The warmed protein samples were subjected to separation by using sodium dodecyl sulfate-polyacrylamide gel electrophoresis (SDS-PAGE), and then transferred onto polyvinylidene difluoride (PVDF; Bio-Rad) membranes soaked in methanol. The membrane was blocked with 5% nonfat milk solution in TBS-T (Tris-buffered saline [TBS] and 0.5% Tween-20) for 1 h. The membrane was incubated overnight with the indicated antibodies at 4 °C and washed thrice with TBS-T. Following washing, the membranes were incubated with horseradish peroxidase (HRP)-conjugated anti-mouse and anti-rabbit secondary antibodies, and the protein bands were visualised using the enhanced luminescent solution (Thermo, 32209). Input and β-actin blots were used as loading control.

Confocal imaging

Transfected cell or sliced SMG tissues were transferred onto cover glasses and fixed with chilled (−20 °C) methanol or 4% paraformaldehyde. The isolated SMG cells were pre-treated with 20 mM NH₄Cl and 100 μM DIDS in 0 Na⁺ solution for intracellular acidification 1 h before fixation. Fixed cells were treated with 5% goat

serum for 1 h at room temperature to block the nonspecific sites. The cells were incubated overnight with primary antibodies (1:50, dilution factor) at 4 °C, followed by washing thrice with PBS. To detect bound antibodies, the cells were treated with goat immunoglobulin G (IgG)-tagged with rhodamine (1:100; Jackson ImmunoResearch, anti-mouse: 115–025-072, anti-rabbit: 111–025-144) or fluorescein isothiocyanate (FITC, 1:100; Jackson ImmunoResearch, anti-mouse: 115–095-071, anti-rabbit: 111–095-003) for 1 h at room temperature. Following incubation, the cells were washed thrice with PBS, and the cover glasses were mounted on glass slides by using Fluoromount-GTM with 4',6-diamidino-2-phenylindole (DAPI) (Electron Microscopy Sciences, Hatfield, PA, 17984–24). The slides were analysed using a LSM 700 Zeiss confocal microscope (Carl Zeiss, Germany) with ZEN software (Carl Zeiss).

Statistical analyses

Data from indicated number of experiments were expressed as the mean ± standard error of the mean (SEM). The statistical differences between the mean values obtained from the two sample groups were analysed using Student's *t*-test parametric. Statistical significance was determined by the analysis of variance in each experiment (**p* < .05).

Results

Basolateral CA12 mutation disrupts the localisation of AQP5 in salivary glands

CA12 is expressed in the basolateral membrane of the acinar and duct cells of the parotid glands⁸. CA12 E143K (E/K) mutation caused reduced secretion of ductal fluids in sealed ducts and inhibited salivation in mice⁸. The total volume of secreted saliva in adenovirus-transduced CA12 E/K was dramatically reduced. In this study, we explored the effect of CA12 and CA12 E/K on the regulation of the water channel AQP5, localised in the luminal membrane as a major water channel in the salivary glands^{11–13} (Supplementary Figure 1). Adenovirus injection was administered to the two SMG and the two parotid glands to enhance the efficacy of viral transfer; the SMG was isolated after 7 days and isolated acinar cells were used for immunostaining. We found mis-localised AQP5 in CA12 E/K-overexpressed salivary glands (Figure 1(A)). To confirm the mis-localisation of AQP5 mediated by CA12 E/K, mKate-CA12WT and -mutant were over-expressed in HEK293 cells with GFP-tagged AQP5. The CA12 E/K mutation mediated localisation of AQP5 in the cytosol, not in the plasma membrane (Supplementary Figure 2). Surface biotinylated assay also revealed about 60% reduced expression of AQP5 in the presence of CA12 E/K (Figure 1(B,C)). Native AQP5 and CA12 were localised in the luminal and basolateral membrane of the SMG, respectively (Figure 1(D)). Although no physical interaction was observed between CA12 and AQP5 by immunoprecipitation assay, it is not known how basolateral CA12 regulates the expression of luminal AQP5.

Intracellular pH modulates AQP5 expression in SMG

Our previous study showed that CA12WT is membrane-associated, whereas CA12 E/K mutant can be observed in the cytosol⁸. CAs generate an acidic component, CO₂⁹, and cytosolic CA12 E/K can be modulated by the intracellular pH (pH_i). We speculated that fluctuations in the basal pH_i level might cause AQP5 localisation. Measurement of the pH_i by BCECF showed that the basal pH of CA12 E/K was about 20% lower than that of CA12WT in HEK293T cells (Figure 2(A)). HEK293T cells were also stained with pH

indicator pHrodo-green. Overexpressed CA12 E/K revealed the enhanced intensity, which represented that CA12 E/K-transfected cells were more acidic (Figure 2(B)). We evaluated the effect of pH_i on the localisation of AQP5. When the isolated SMG cells were treated with NH₄Cl, the initial pH_i was alkalinised by the diffusion of NH₃ and subsequently acidified by NH₄⁺ influx. In the presence of amiloride, an inhibitor of amiloride-sensitive NHE and NBC¹⁴, the pH_i moved to the acidic end, and the recovery response was delayed, indicating the inhibition of H⁺ extrusion and HCO₃⁻ uptake in order to maintain the acidic pH_i (Figure 2(C)). We also evaluated the surface expression of AQP5 by using the biotinylated assay at acidified pH_i. The isolated SMG cells were stimulated in DIDS, followed by NH₄Cl stimulation. The surface expression of AQP5 was diminished by acidosis (Figure 2(D)). Additionally, the isolated SMG cells were administered NH₄Cl, and subsequently exposed to DIDS in Na⁺-free solution to acidify the pH_i, and AQP5 expression was studied using confocal microscopy. Luminal AQP5 expression of SMG acinar cells was almost absent under acidic conditions (Figure 2(E)). These results showed that pH_i modulates the membrane expression of AQP5 in SMG. Stimulation of the salivary gland cells results in bulk water efflux and can be observed as cell shrinkage¹⁵, whereas water influx results in cell swelling. AQP5 has been known as an osmosensor¹⁶. To evaluate the volume regulation of AQP5 in salivary glands, isolated SMG acinar cells were stimulated in a hypotonic (215 mOsm) solution, and the volume change was measured using the calcein-AM fluorescent technique. Shrinkage of SMG cells and increase in fluorescence intensity were observed when moved to a hypertonic solution, while swelling of SMG cells and decrease in fluorescence intensity were elicited when moved to a hypotonic solution (Supplementary Figure 3A). The mRNA and protein levels of AQP5 at different levels of tonicity did not alter the expression level (Supplementary Figure 3(B,C)). We evaluated the volume regulation of AQP5 under acidified conditions. The isolated SMG cells showed an increase in cell swelling under hypotonic stimulation (Figure 2(F,G)). These results suggest that intracellular acidification reduced the expression of AQP5 and subsequent volume dysregulation. Mutation of CA12 also provided the acidic environment in cytosolic area (Figure 2(H)).

CA12 E/K mutation modulates the volume regulation of AQP5

In response to inflammation, the transport of salt and water is decreased to provide physiological protection^{17,18}. The stimulation of TNF-α, a primary component of inflammation, reduces saliva secretion. Isolated SMG cells were pre-treated with TNF-α to confirm the volume regulation occurring during inflammation. We found that TNF-α mediated the increase in cell swelling through the attenuation of AQP5 (Figure 3(A,B)). We administered the CA inhibitor acetazolamide, a well-known diuretic^{19,20}. Acetazolamide inhibited the swelling property of cells (Figure 3(A,B)). To confirm the effect of acidification and acetazolamide stimulation on the swelling property of cells, isolated SMG cells were stimulated using the cholinergic agonist carbamyl chlorine chloride (carbachol) to activate fluid secretion (Figure 3(C)). Stimulation of fluid secretion by carbachol results in large water efflux and cell shrinkage in the salivary glands¹⁵. Isolated SMG cells were found to shrink by carbachol stimulation. However, in the presence of intracellular acidification and TNF-α stimulation, isolated SMG cells did not shrink and the volume was maintained (Figure 3(D)), suggesting that the loss of AQP5 caused volume dysregulation in the presence of the agonist of fluid secretion.

To determine whether CA12 E/K mutation mediates volume dysregulation, we performed volume measurement in CA12 and

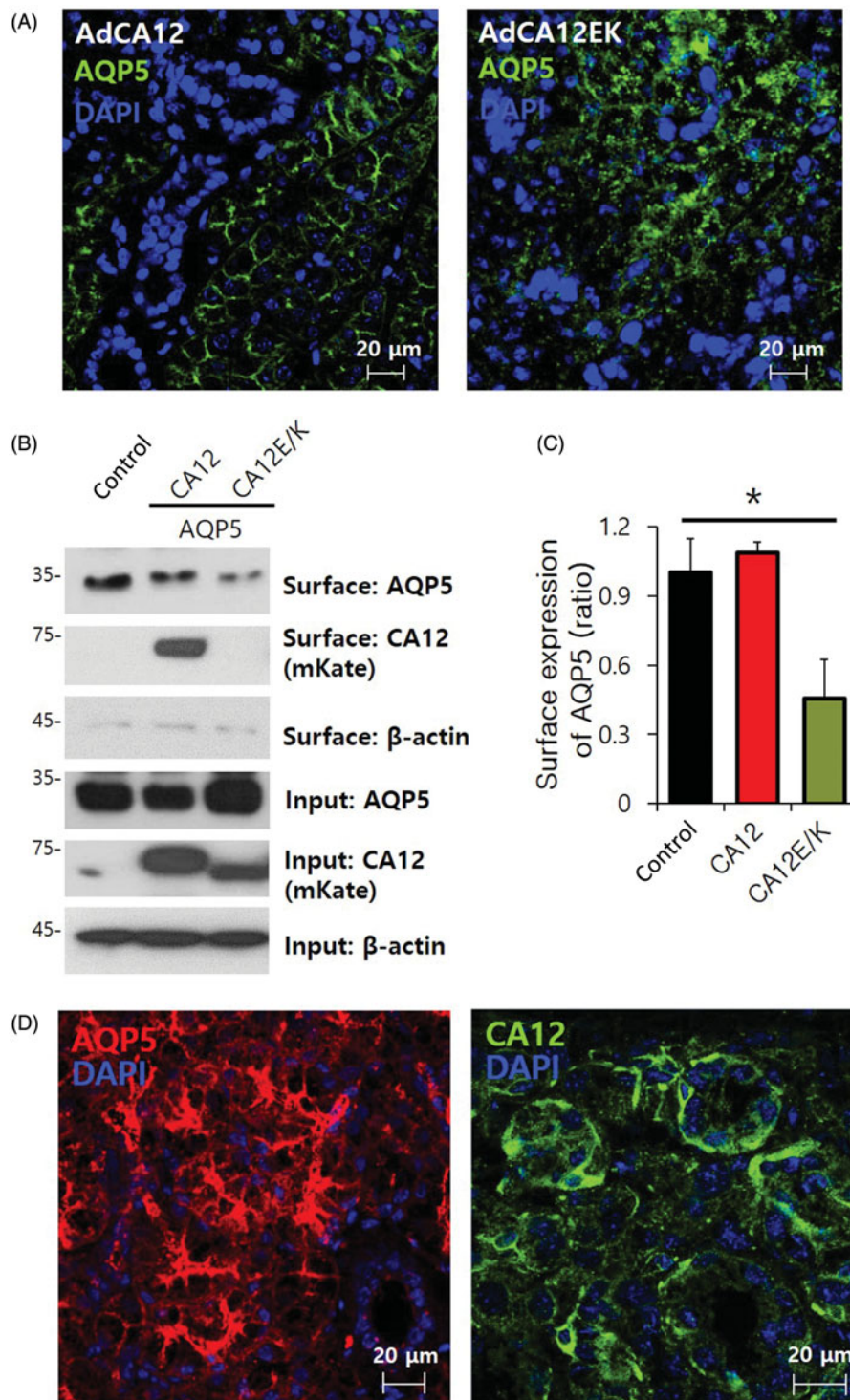


Figure 1. Basolateral CA12 mutation disrupts the localisation of AQP5. (A) Localisation of AQP5 (green) in the submandibular gland (SMG) after delivering the adenoviral CA12 or CA12 E/K. (B) Effect of mKate-CA12 and mKate-CA12 (E/K) on the surface expression of AQP5 in transfected HEK293T cells. (C) The columns represent the mean \pm standard error of mean (SEM) of AQP5 surface expression ($p < .05$, indicated by an asterisk, $n = 4$). (D) Native expression of AQP5 (red) and CA12 (green) in mouse SMG.

AQP5-overexpressed HEK293T cells. The volume of CA12-WT-enriched cells was not modulated by the hypotonic stimulation (Figure 3(E)). The hypotonic solution elicited an increase in the cell swelling property in the presence of CA12 E/K mutation, suggesting dysfunction of the cytosolic AQP5 induced by CA12 E/K mutation in response to hypotonicity (Figure 3(F)). These results suggest that the endogenous acidosis caused by inflammatory signals, including CA12 E/K mutation, mediate concomitant

internalised expression of AQP5 and obviously dysregulate the volume in salivary glands.

AQP5 is functionally associated with the transepithelial transporter AE2

To the best of our knowledge, AQP-mediated fluid movement is regulated by an osmotic gradient²¹. To provide a basis for

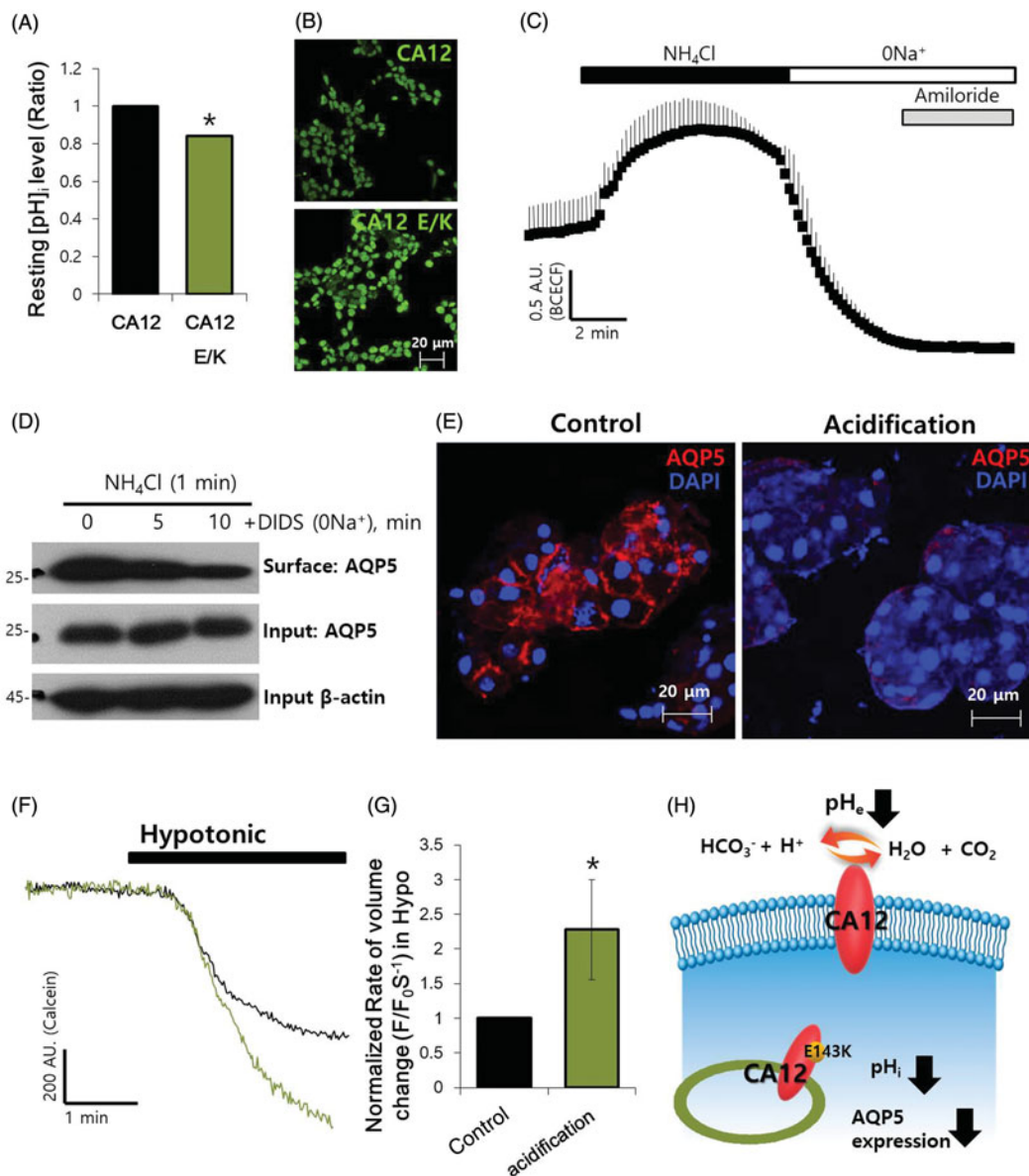


Figure 2. Intracellular pH modulates AQP5 expression in SMG. (A) Analysis of the intracellular resting pH level (ratio) of HEK293T cells transfected with CA12 or CA12 E/K ($p < .05$, indicated by an asterisk, $n = 7$). (B) pHrodo staining (green) images of HEK293T cells transfected with CA12 or CA12 E/K. Enhanced intensity represented acidic pH. (C) pH changes during the NH₄⁺-pulse acidification technique. Upon removal of 10 mM NH₄Cl solution after the influx of NH₄⁺, the cells were acidified using the remaining H⁺. Amiloride (500 μM) was used to inhibit Na⁺ reabsorption through the Na⁺ channel. (D) Surface expression of AQP5 during intracellular acidification with 10 mM NH₄Cl and 100 μM DIDS in 0Na⁺ solution (Na⁺-free solution). (E) Changes in AQP5 localisation during intracellular acidification with 10 mM NH₄Cl and 100 μM DIDS in 0Na⁺ solution for the indicated time period. SMG acinar cells were stained with DAPI (blue) to indicate the presence of AQP5 (red). (F) Cells were stimulated in a hypotonic (215 mOsm) solution, and the change in volume was measured using 2 μM calcein-AM. The changes in the volume of acidification-induced SMG acinar cells (using 10 mM NH₄Cl and 100 μM DIDS in 0Na⁺ solution for 30 min) were measured. The isolated mouse SMG acinar cells were stimulated in the hypotonic (215 mOsm) solution. (G) The columns show the mean ± SEM of the normalised rate of volume change ($F/F_0 \cdot S^{-1}$), $p < .05$, indicated by an asterisk, $n = 5$). (H) Schematic illustration of function and trafficking of CA12 wild type and E/K mutant.

understanding the role of AQP5 in transepithelial ion transport, we examined whether these solute transporters modulate volume regulation of AQP5 in the salivary glands. Various transporters are expressed and involved in salivary function. Among them, AE2 was found to be modulated by CA12, in our previous study⁸. The AE2 localised in the plasma membrane and several dots of AE2 co-localised with the tight junction marker ZO-1 (Figure 4(A,B)). The direct interaction of membrane proteins indicate that these proteins are functionally linked¹⁶. We confirmed the protein–protein interaction of AE2 and AQP5 in SMG cells and an overexpressed system in HEK293T cells (Figure 4(C), Supplementary Figure 4A). The volume regulation of AQP5 was independent of AE2, whereas AE2-overexpressed cells showed enhanced swelling property (Figure 4(D)). We

next evaluated the changes of pH_i by using the BCECF-AM to measure the HCO₃⁻-transporting activity. Interestingly, AE2 activity was enhanced in the presence of AQP5 (Figure 4(E)).

AQP5 is functionally associated with the transepithelial transporter NKCC1

To assess the relationship between transepithelial ion transport and volume regulation, we confirmed that another solute-transporting system NKCC1 is physiologically associated with AQP5. NKCC1 and AQP5 co-localised in the lumen of acinar cells and interacted with each other (Figure 5(A–C)). We confirmed the protein–protein interaction of NKCC1 and AQP5 in an overexpressed

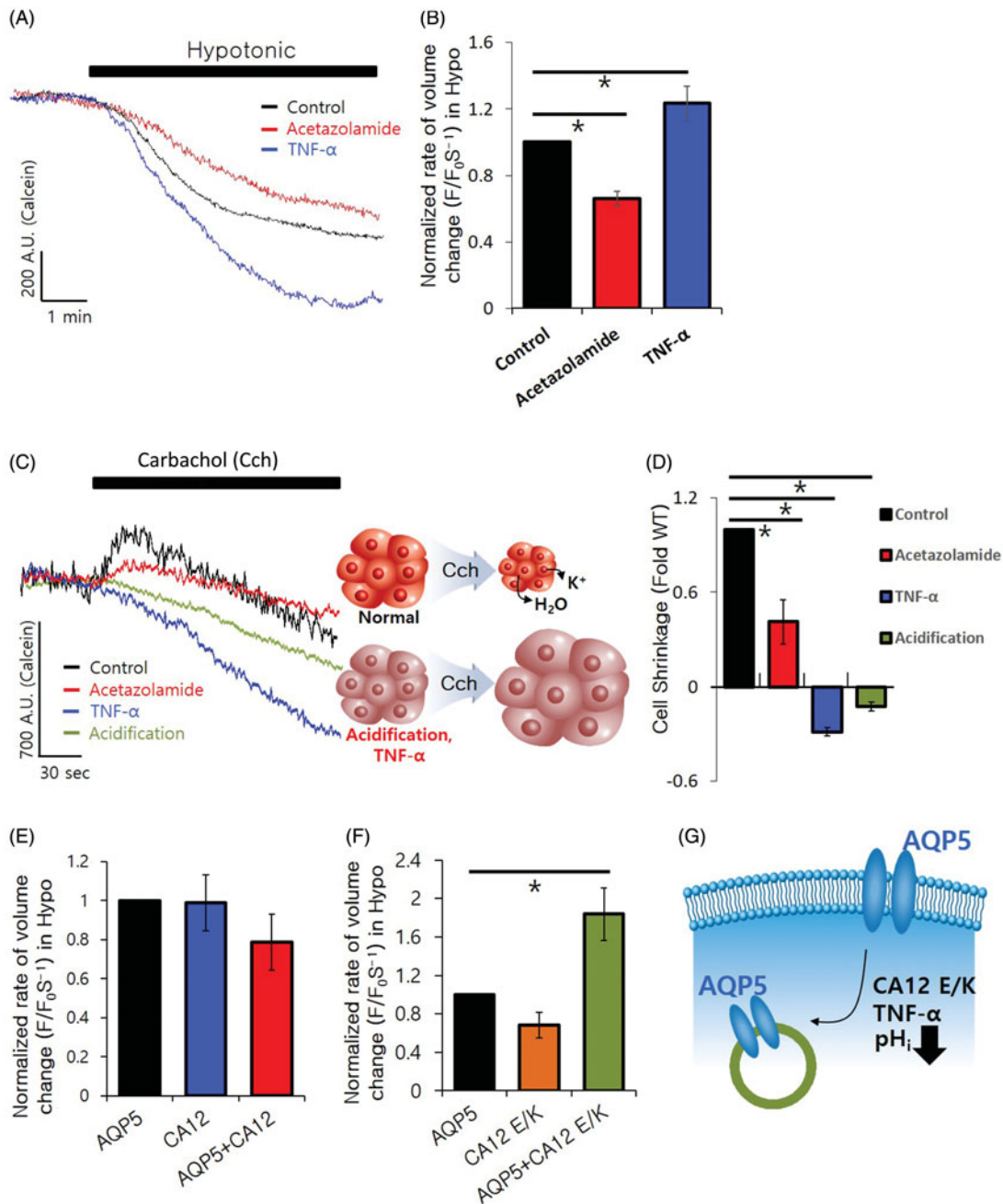


Figure 3. CA12 E/K mutation modulates volume regulation of AQP5. (A) Volume regulation of AQP5 on stimulation with a hypotonic (215 mOsm) solution pre-treated with 100 μ M acetazolamide and 10 ng/mL TNF- α for 1 h. (B) The columns represent the mean \pm SEM of the normalised rate of volume change ($F/F_0 \cdot S^{-1}$, $p < .05$, indicated by an asterisk, $n = 4$). (C) Volume regulation of SMG on stimulation of 10 μ M carbachol with and without treatment with 100 μ M acetazolamide and 10 ng/mL TNF- α for 1 h, followed by acidification. (D) The columns represent the mean \pm SEM of the fold changes of cell shrinkage after carbachol treatment ($p < .05$, indicated by an asterisk, $n = 3$). (E and F) Volume regulation of AQP5 by stimulation in a hypotonic (215 mOsm) solution with and without CA12 and CA12 E/K. The columns represent the mean \pm SEM of normalised rate of volume change ($F/F_0 \cdot S^{-1}$, $p < .05$, indicated by asterisk, $n = 6$). (G) Schematic illustration of cross talk mechanism to affect AQP5 localisation.

system of HEK293T cells (Supplementary Figure 4B). Volume regulation of AQP5 was maintained with and without NKCC1 (Figure 5(D)). AQP5 also enhanced NKCC activity, like AE2 activity (Figure 5(E)). It is noted that the solute transporters-overexpressed system, including AE2 and NKCC1, which only exists in native water channels, enhanced the swelling property (Figures 4(D) and 5(D)). Collectively, these results suggest that the activities of AE2 and NKCC were supported by AQP5 for osmotic regulation, suggesting that the membrane expression of AQP5 affects the swelling property in the presence of solute influx. Normal expression of CA12 also provides HCO₃⁻ consumption and water source to transporters

and AQP5, respectively (Figure 5(F)). The Cl⁻-HCO₃⁻ exchanger AE2 and solute carrier transporter family 26 (SLC26) A6 are abundantly expressed in the plasma and luminal membranes of salivary glands, respectively, as acid loaders²². Another luminal protein SLC26A6 was independent of AQP5, with no changes in activity or protein-protein interaction (Supplementary Figure 5).

Discussion

Dysregulated volume homeostasis in the salivary glands plays an important role in the secretion of fluid and saliva. AQP5 is

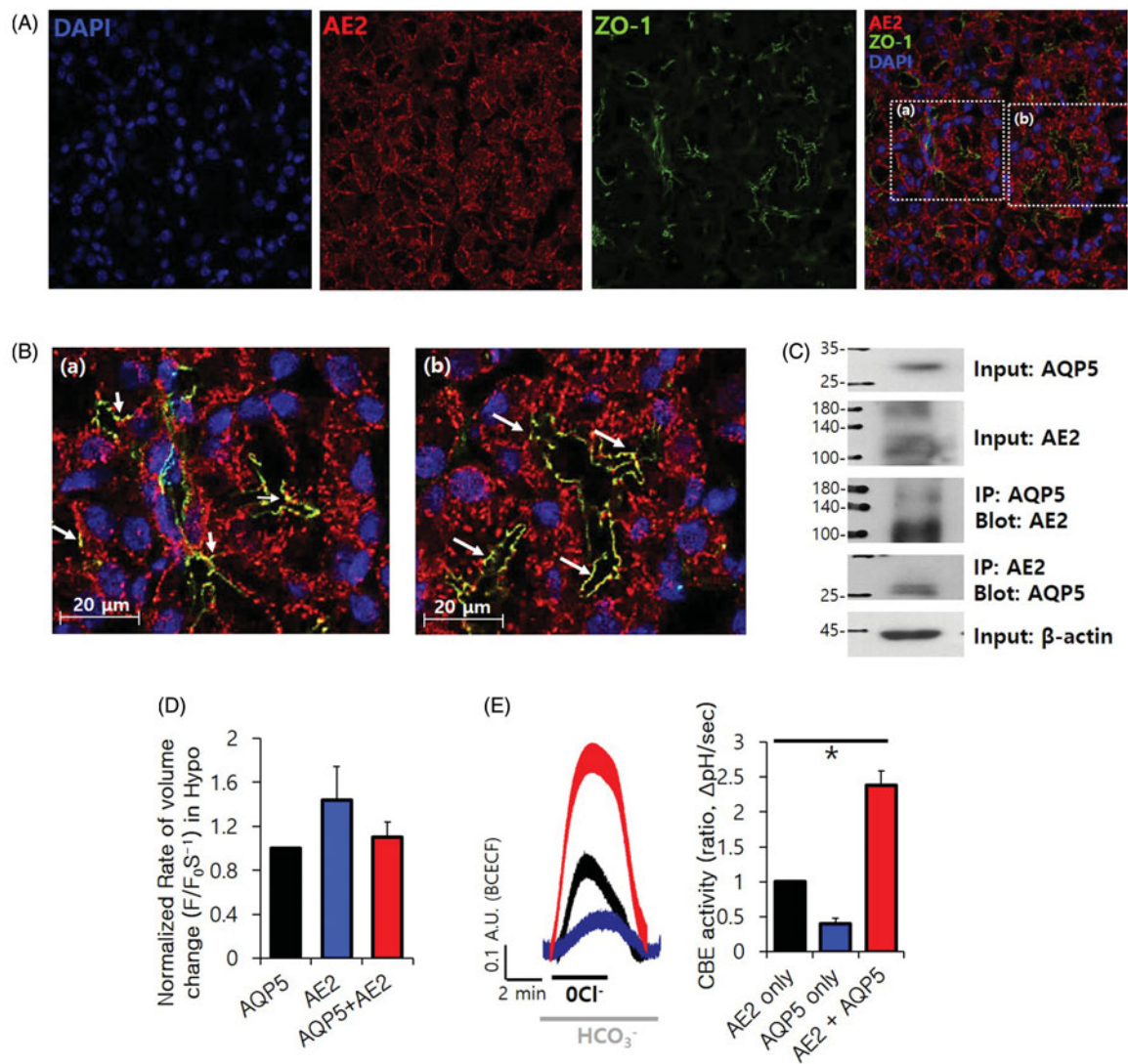


Figure 4. AQP5 is functionally associated with the transepithelial transporter AE2 (A) Native localisation of DAPI (blue), AE2 (red), and ZO-1 (green) in the mouse SMG. (B) High-magnification images of the co-staining areas in (a) and (b). (C) Co-immunoprecipitation (Co-IP) of AE2 and AQP5 in isolated SMG. (D) Volume regulation of AQP5 with and without AE2 by hypotonic stimulation in HEK293T cells. The columns represent the mean \pm SEM of the normalised rate of volume change ($F/F_0 \cdot S^{-1}$, $n = 5$). (E) Effect of AQP5 on the chloride/bicarbonate exchanger (CBE) activity of AE2-transfected HEK293T cells. The columns represent the mean \pm SEM of CBE activity ($p < .05$, indicated by an asterisk, $n = 3$).

involved in transcellular water permeability and is a dominant water channel in the epithelia of the salivary and lacrimal glands, and the lung alveoli^{1,2}. Appropriate expression of AQP5 in the luminal membrane aids homeostatic volume regulation. In this study, we found that the regulatory factors, endogenous acidification, inflammatory factors, and CA12 E/K mutation, all mediate the dysregulation of AQP5. Basically, decreased AQP5 expression might reduce water intake. However, enhanced cell swelling by decreased AQP5 expression in the plasma membrane might indicate ion transporter-mediated volume dysregulation in the absence of AQP5. Movement of solutes by ion transporters is accompanied by the movement of water through AQP5. Intrinsic modulation by acidosis might affect the expression of AQP5 in the plasma membrane.

The present findings show that the effect of the CA12 E/K mutation, expressed in the cytosol, mediated the mistargeting of AQP5. The membrane-associated CAs promote extracellular acidification²³. The mislocalised CA12 E/K in the cytosol can mediate aberrant pH_i homeostasis. Our results provide strong evidence that AQP5 expression is sensitive to pH_i . Abnormal localisation of

CA12 E/K mutation generates an acidic intracellular environment, and pH_i -sensitive components such as AQP5 can be affected. We speculated that reduced expression of AQP5 by CA12 E/K provided an ion transporter-rich state in the plasma membrane. The movement of solutes by ion transporters such as AE2 and NKCC1 can be acutely diluted by water to prevent osmotic imbalance. The cross-talk between ion transporters and AQP5 might maintain complementary volume regulation. The osmotic maintenance of AQP5 with transepithelial ion transporters is a typical process in volume regulation. Disruption of AQP5 expression by CA12 E/K can provide another candidate mechanism for reduced salivary volume.

Human CA12 mutation, which results in autosomal recessive hereditary hyperchlorhidrosis, reduces CA activity and leads to an autosomal-recessive phenotype, including excessive Cl^- secretion in sweat²⁴. CAs are involved in the reverse reaction involving CO_2 and water to release H^+ and HCO_3^- ⁹. Mammalian CAs are identified in the cytoplasmic (CA2 and CA7), mitochondrion-associated (CA5), secretory (CA6), and plasma membrane-associated (CA4, CA9, CA12, and CA14)

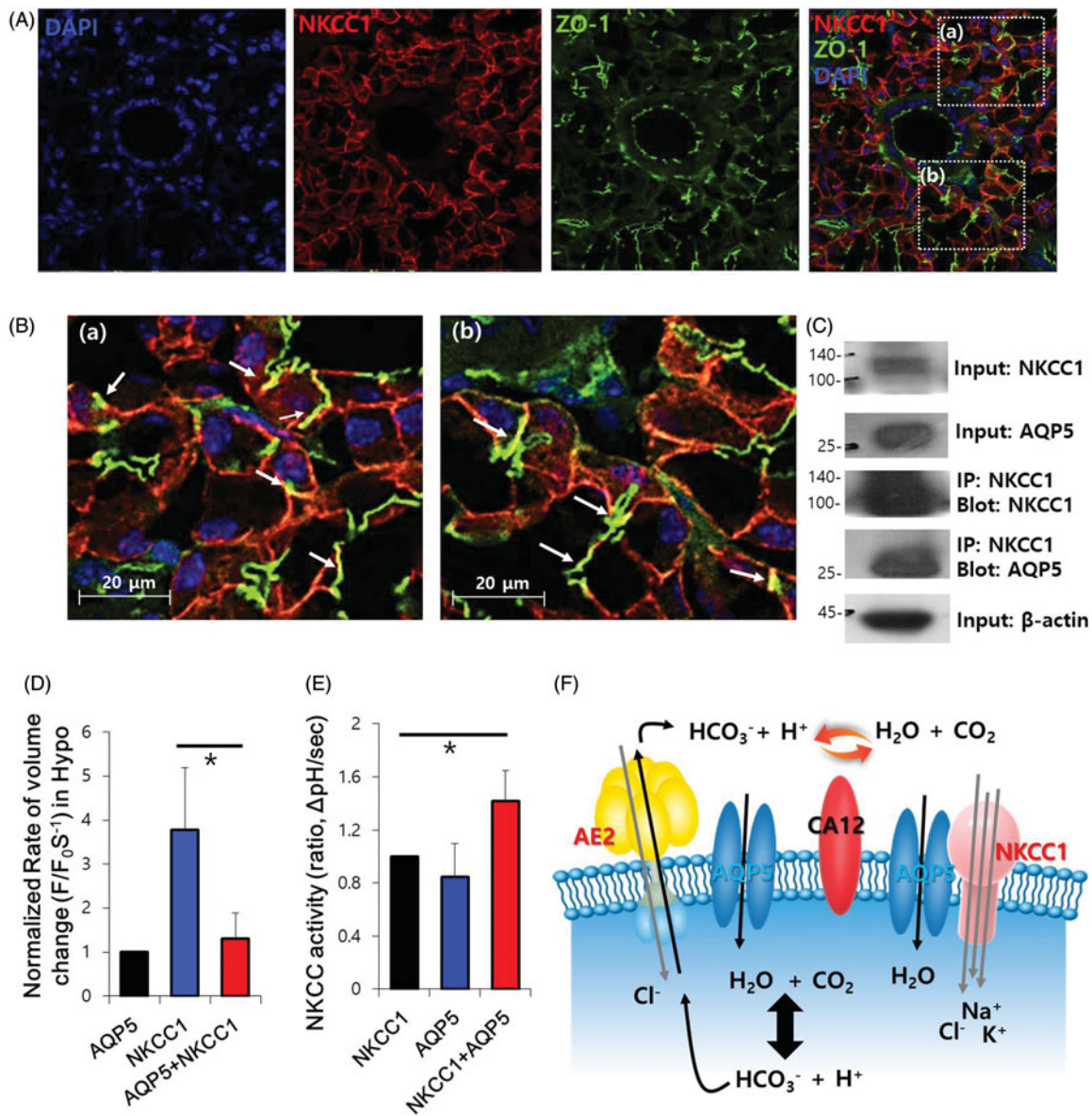


Figure 5. AQP5 is functionally associated with the transepithelial transporter NKCC1. (A) Native localisation of DAPI (blue), NKCC1 (red), and ZO-1 (green) in the mouse SMG. (B) High-magnification images of the co-staining areas in (a) and (b). (C) Co-IP of NKCC1 and AQP5 in SMG. (D) Volume regulation of AQP5 with and without NKCC1 by hypotonic stimulation in HEK293T cells. The columns represent the mean \pm SEM of the normalised rate of volume change ($F/F_0 \cdot S^{-1}$, $p < .05$, indicated by an asterisk, $n = 5$). (E) Effect of AQP5 on the NKCC1 activity of NKCC1-transfected HEK293T cells. The columns represent the mean \pm SEM of NKCC activity ($p < .05$, indicated by an asterisk, $n = 3$). (F) Schematic illustration of cross talk mechanism between AQP5 and the transepithelial transporters AE2 and NKCC1.

enzymes⁹. The plasma membrane-localised CAs functionally couple with and regulate the activity of HCO_3^- transporters, including NBCe1 and AE2^{8,25,26}. Although the functional role of CAs in fluid and HCO_3^- secretion, including AQP5, is obvious, the functional and physiological interactions between other type of CAs and AQP5 are still unclear.

In this study, we, for the first time, to the best of our knowledge, provided direct evidence of the modulatory role of CA12 on AQP5 expression. Dysregulation of AQP5 by the CA12 deficiency caused by CA12 E/K mutation might involve excessive Cl^- secretion, resulting in hyperchlorhidrosis in humans. In addition, for the cancer treatment, several blockades of oncogene CA12 have been developed^{27–29}. Accordingly, intracellular acidification, inflammation, or application of blockades of oncogene CA12 should be induced osmotic dysregulation in case of volume-sensitive exocrine glands such as the salivary glands, which abundantly express AQP5.

Disclosure statement

The authors declare that they have no conflicts of interest with the contents of this article.

Funding

This work was supported by the National Research Foundation of Korea (NRF) grant funded by the Korean Government [NRF-2017 R1D1A1B03029570 (JHH)], [NRF-2016 R1A5A2008630 (DMS)].

References

- Matsuzaki T, Suzuki T, Koyama H, et al. Aquaporin-5 (aqp5), a water channel protein, in the rat salivary and lacrimal glands: Immunolocalization and effect of secretory stimulation. *Cell Tissue Res* 1999;295:513–21.

2. Hoffert JD, Leitch V, Agre P, King LS. Hypertonic induction of aquaporin-5 expression through an erk-dependent pathway. *J Biol Chem* 2000;275:9070–7.
3. Ma T, Song Y, Gillespie A, et al. Defective secretion of saliva in transgenic mice lacking aquaporin-5 water channels. *J Biol Chem* 1999;274:20071–4.
4. Delporte C, Bryla A, Perret J. Aquaporins in salivary glands: from basic research to clinical applications. *Int J Mol Sci* 2016;17:166.
5. Jensen HH, Login FH, Park JY, et al. Immunohistochemical evaluation of activated ras and rac1 as potential downstream effectors of aquaporin-5 in breast cancer in vivo. *Biochem Biophys Res Commun* 2017;493:1210–6.
6. He Z, Dong W, Hu J, Ren X. Aqp5 promotes hepatocellular carcinoma metastasis via nf-kappab-regulated epithelial-mesenchymal transition. *Biochem Biophys Res Commun* 2017;490:343–8.
7. Ren Y, Lu H, Reinach PS, et al. Hyperosmolarity-induced aqp5 upregulation promotes inflammation and cell death via jnk1/2 activation in human corneal epithelial cells. *Sci Rep* 2017;7:4727.
8. Hong JH, Muhammad E, Zheng C, et al. Essential role of carbonic anhydrase xii in secretory gland fluid and HCO_3^- secretion revealed by disease causing human mutation. *J Physiol* 2015;593:5299–312.
9. McKenna R, Frost SC. Overview of the carbonic anhydrase family. *Sub-Cell Biochem* 2014;75:3–5.
10. Gresz V, Kwon TH, Hurley PT, et al. Identification and localization of aquaporin water channels in human salivary glands. *Am J Physiol Gastrointest Liver Physiol* 2001;281:G247–54.
11. Gresz V, Kwon TH, Gong H, et al. Immunolocalization of aqp-5 in rat parotid and submandibular salivary glands after stimulation or inhibition of secretion in vivo. *Am J Physiol Gastrointest Liver Physiol* 2004;287:G151–61.
12. Verkman AS, Matthay MA, Song Y. Aquaporin water channels and lung physiology. *Am J Physiol Lung Cell Mol Physiol* 2000;278:L867–79.
13. Kreda SM, Gynn MC, Fenstermacher DA, et al. Expression and localization of epithelial aquaporins in the adult human lung. *Am J Respir Cell Mol Biol* 2001;24:224–34.
14. Li J, Koo NY, Cho IH, et al. Expression of the $\text{Na}^+/\text{HCO}_3^-$ cotransporter and its role in phi regulation in guinea pig salivary glands. *Am J Physiol Gastrointest Liver Physiol* 2006;291:G1031–40.
15. Teos LY, Zhang Y, Cotrim AP, et al. IP3R deficit underlies loss of salivary fluid secretion in Sjogren's syndrome. *Sci Rep* 2015;5:13953.
16. Procino G, Milano S, Tamma G, et al. Co-regulated pendrin and aquaporin 5 expression and trafficking in type-b intercalated cells under potassium depletion. *Cell Physiol Biochem* 2013;32:184–99.
17. Weidenfeld S, Kuebler WM. Cytokine-regulation of $\text{Na}^+/\text{K}^+/\text{Cl}^-$ cotransporter 1 and cystic fibrosis transmembrane conductance regulator-potential role in pulmonary inflammation and edema formation. *Front Immunol* 2017;8:393.
18. Hosoi K. Physiological role of aquaporin 5 in salivary glands. *Pflugers Arch* 2016;468:519–39.
19. Nguyen HV, Stuart-Tilley A, Alper SL, Melvin JE. $\text{Cl}^-/\text{HCO}_3^-$ exchange is acetazolamide sensitive and activated by a muscarinic receptor-induced $[\text{Ca}^{2+}]_i$ increase in salivary acinar cells. *Am J Physiol. Gastrointestinal Liver Physiol* 2004;286:G312–20.
20. Imiela T, Budaj A. Acetazolamide as add-on diuretic therapy in exacerbations of chronic heart failure: A pilot study. *Clin Drug Investig* 2017;37:1175–81.
21. Zhang J, Yan M, Gu W, et al. Downregulation of aquaporins (aqp1 and aqp5) and $\text{Na},\text{K}\text{-ATPase}$ in porcine reproductive and respiratory syndrome virus-infected pig lungs. *Inflammation* 2018;41:1104–14.
22. Boron WF, Chen L, Parker MD. Modular structure of sodium-coupled bicarbonate transporters. *J Exp Biol* 2009;212:1697–706.
23. Bouchareb R, Cote N, Marie Chloe B, et al. Carbonic anhydrase xii in valve interstitial cells promotes the regression of calcific aortic valve stenosis. *J Mol Cell Cardiol* 2015;82:104–15.
24. Feldshtein M, Elkrinawi S, Yerushalmi B, et al. Hyperchlorhidrosis caused by homozygous mutation in CA12, encoding carbonic anhydrase XII. *Am J Hum Genet* 2010;87:713–20.
25. Becker HM, Klier M, Deitmer JW. Carbonic anhydrases and their interplay with acid/base-coupled membrane transporters. *Sub-Cell Biochem* 2014;75:105–34.
26. Orłowski A, De Giusti VC, Morgan PE, et al. Binding of carbonic anhydrase IX to extracellular loop 4 of the $\text{NBCe1 Na}^+/\text{HCO}_3^-$ cotransporter enhances NBCe1 -mediated HCO_3^- influx in the rat heart. *Am J Physiol Cell Physiol* 2012;303:C69–80.
27. Guler O, Simone G, Supuran C. Drug design studies of the novel antitumor targets carbonic anhydrase ix and xii. *Curr Med Chem* 2010;17:1516–26.
28. Singh S, Lomelino CL, Mboge MY, et al. Cancer drug development of carbonic anhydrase inhibitors beyond the active site. *Molecules* 2018;23:1045 (22 pages).
29. Waheed A, Sly WS. Carbonic anhydrase xii functions in health and disease. *Gene* 2017;623:33–40.